Supporting Information

Quantitatively Unraveling the Redox Shuttle of Spontaneous Oxidation/Electroreduction of CuO_x on Silver Nanowires Using *in Situ* X-ray Absorption Spectroscopy

Chia-Jui Chang,[a] *Sung-Fu Hung,*[a] *Chia-Shuo Hsu,*[a] *Hsiao-Chien Chen,*[a] *Sheng-Chih Lin,*[a] *Yen-Fa Liao,*[b] *Hao Ming Chen*[a,b*]

[a] *Department of Chemistry, National Taiwan University, Taipei 106, Taiwan*

[b] *National Synchrotron Radiation Research Center, Hsinchu 300, Taiwan*

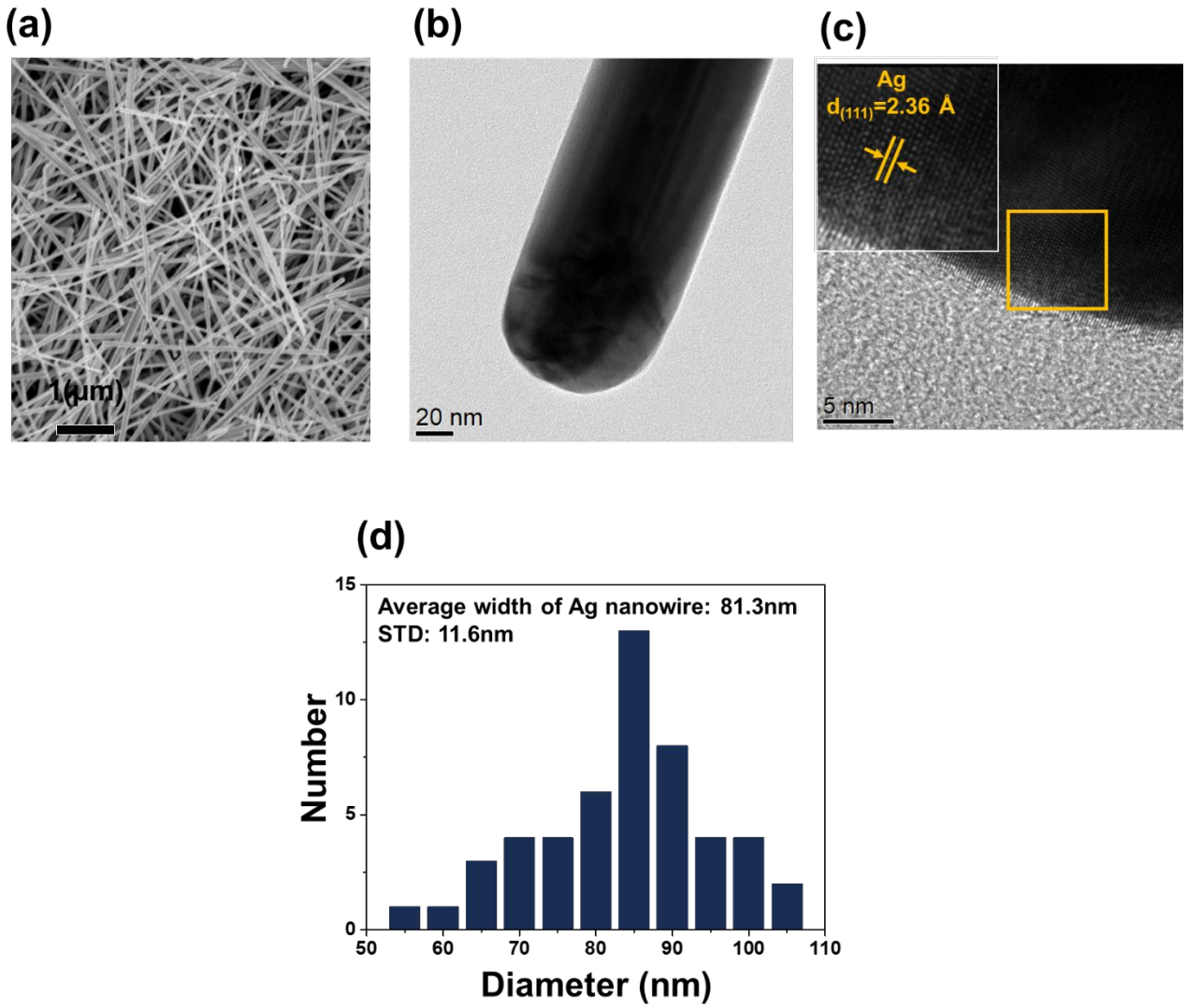

Figure S1. Typical SEM (a) and TEM (b) images of Ag nanowires. (c) HRTEM image of the Ag nanowire. (d) Diameter of silver nanowires. The diameter was determined as follows: Fifty silver nanowires were chosen at random and Image J was used to measure the diameter.

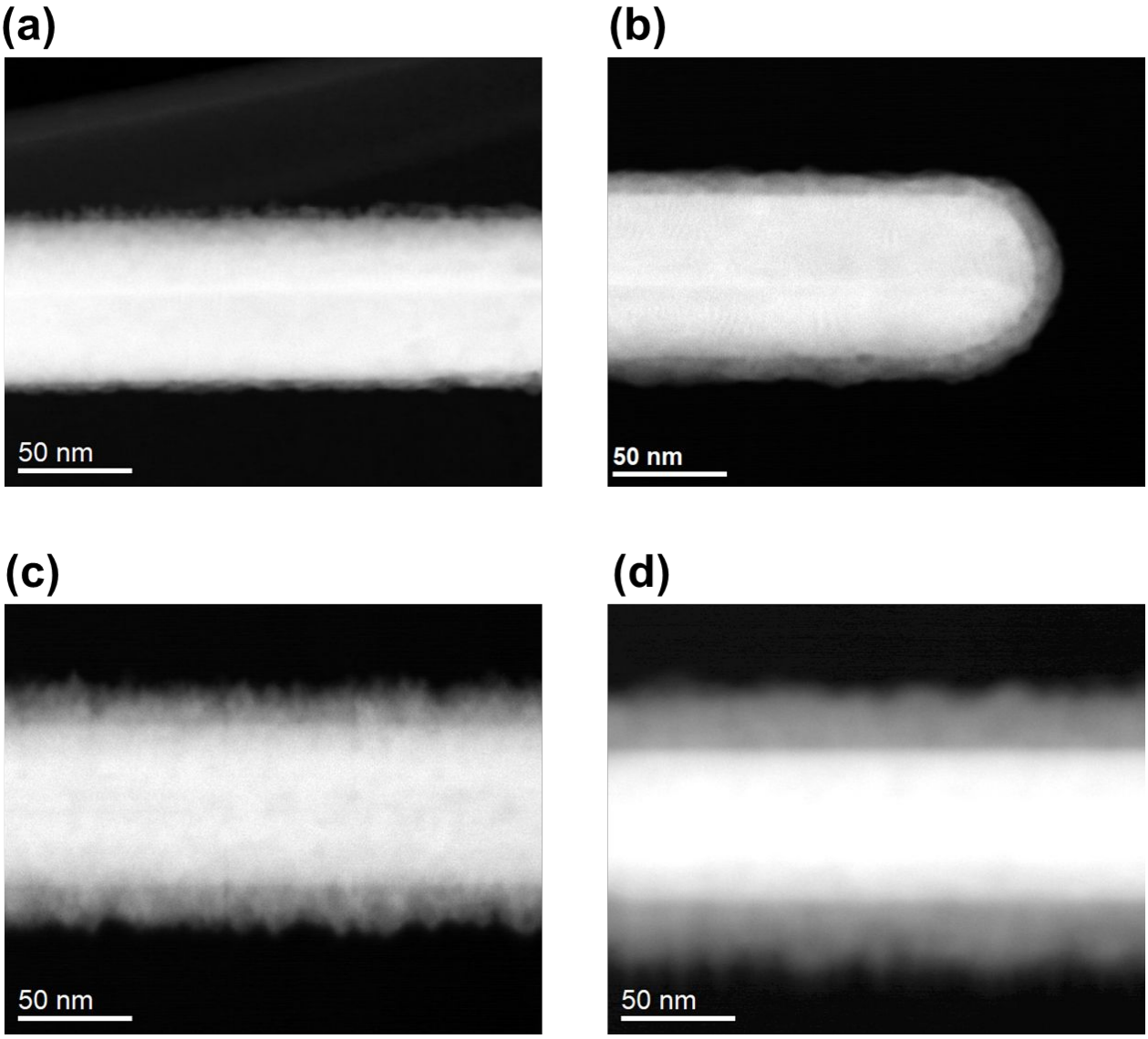

Figure S2. Scanning transmission electron microscopy-high angle annular dark field (STEM-HAADF) images of each sample. Ag@CuO_x-4 (a), Ag@CuO_x-10 (b), Ag@CuO_x-24 (c), and Ag@CuO_x-32 (d).

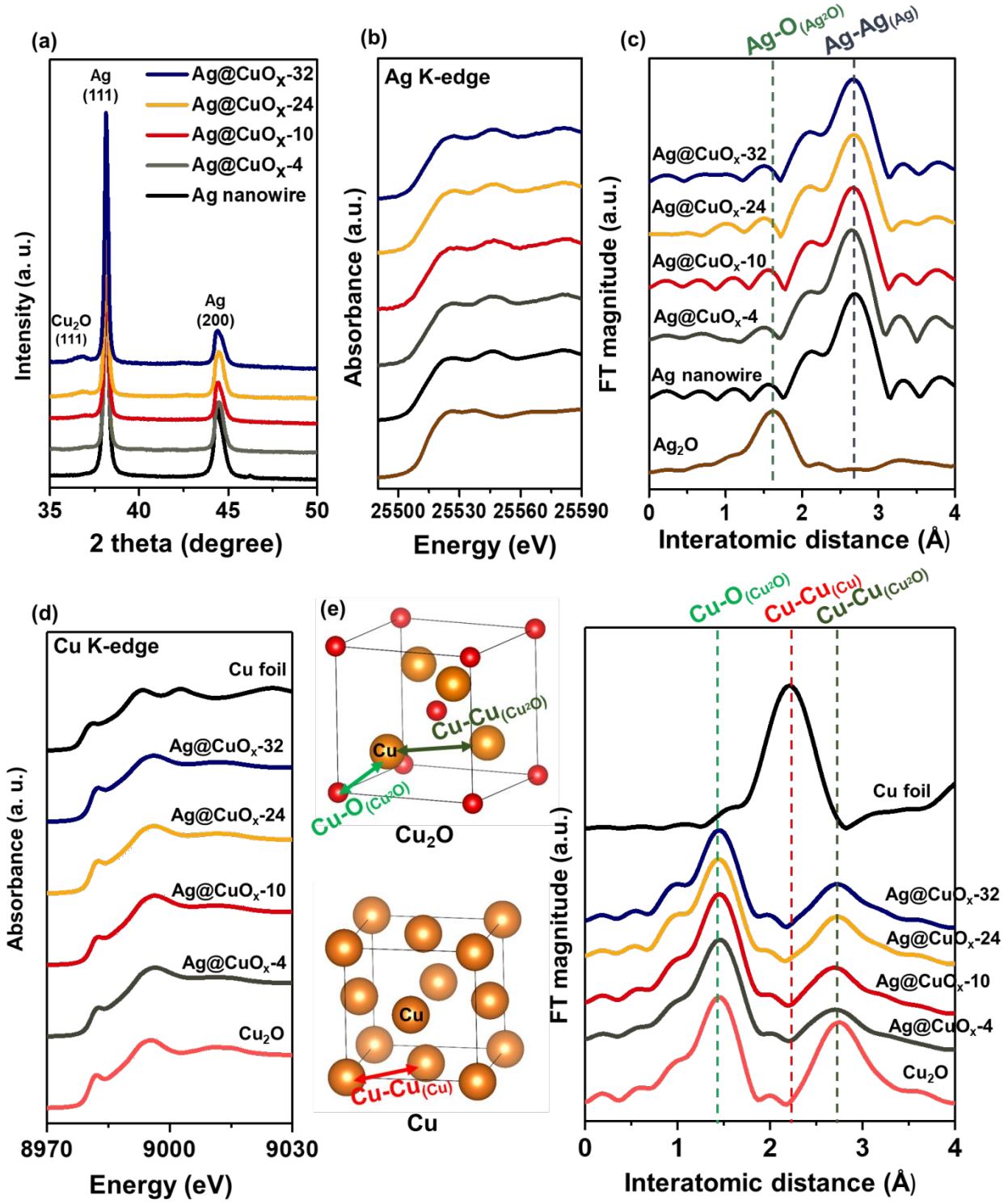

Figure S3. XRD pattern (a), Ag K-edge XANES spectra (b), Ag K-edge EXAFS spectra (c), Cu K-edge XANES spectra (d), and Cu K-edge EXAFS spectra (e) of the Ag@CuO_x-4, Ag@CuO_x-10, Ag@CuO_x-24, and Ag@CuO_x-32 samples.

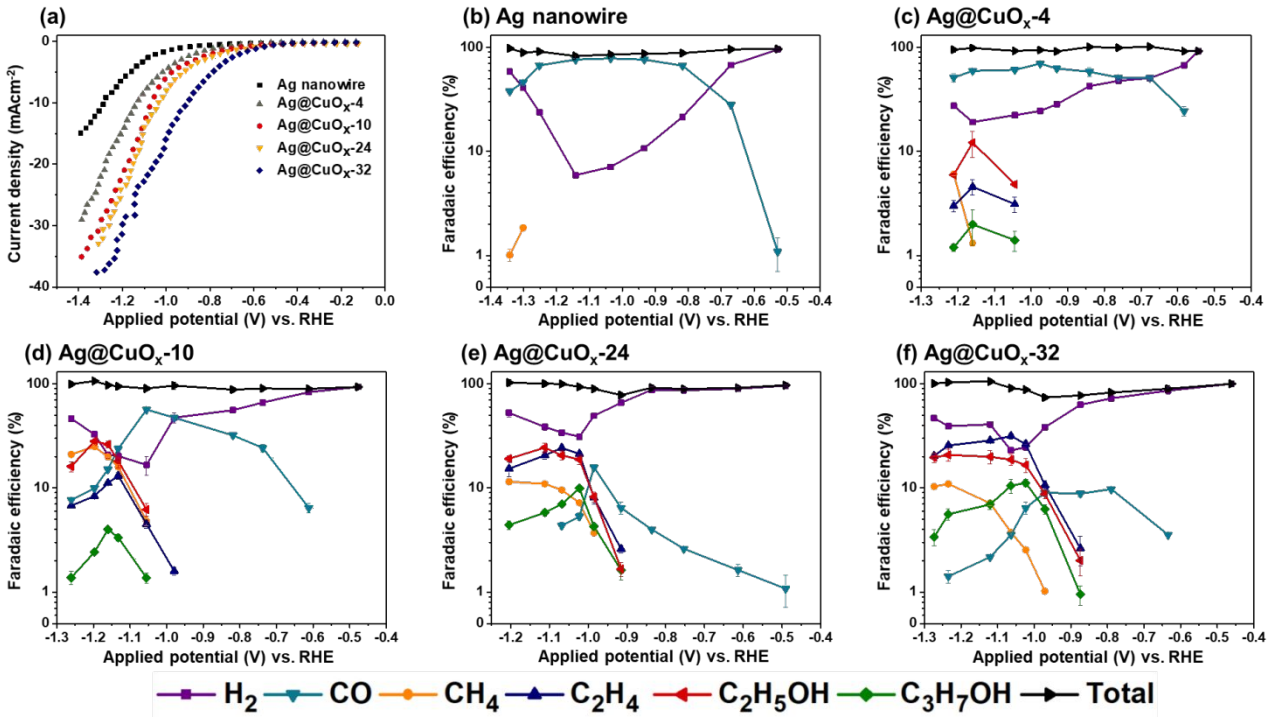

Figure S4. Electrochemical CO_2 reduction for each sample. (a) LSV under saturated CO_2 in 0.1 M $KHCO_3$. (b-f) Faradaic efficiency (FE) as a function of potential for the Ag nanowire, Ag@CuO_x-4, Ag@CuO_x-10, Ag@CuO_x-24, and Ag@CuO_x-32 samples.

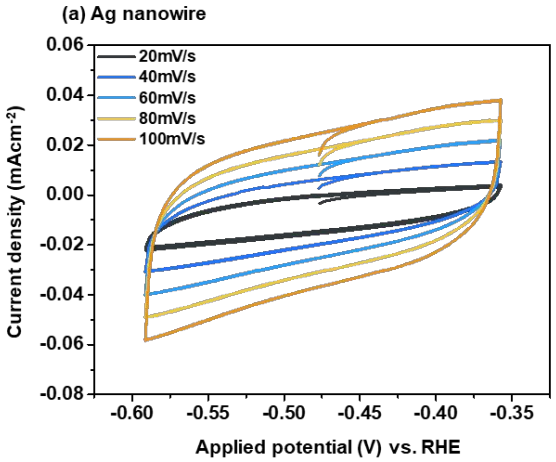
(a) Ag nanowire
20mV/s
40mV/s
60mV/s
80mV/s
100mV/s
Current density (mAcm-2)
Applied potential (V) vs. RHE

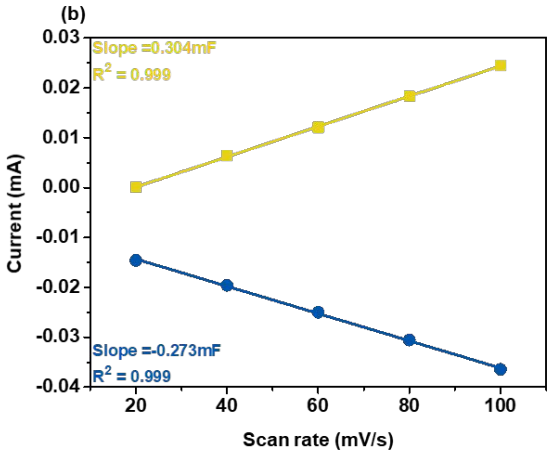
(b)
Slope =0.304mF
R2 = 0.999
Slope =-0.273mF
R2 = 0.999
Current (mA)
Scan rate (mV/s)

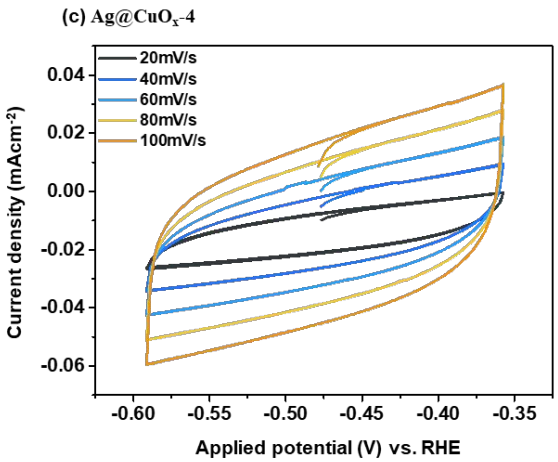
(c) Ag@CuOx-4
20mV/s
40mV/s
60mV/s
80mV/s
100mV/s
Current density (mAcm-2)
Applied potential (V) vs. RHE

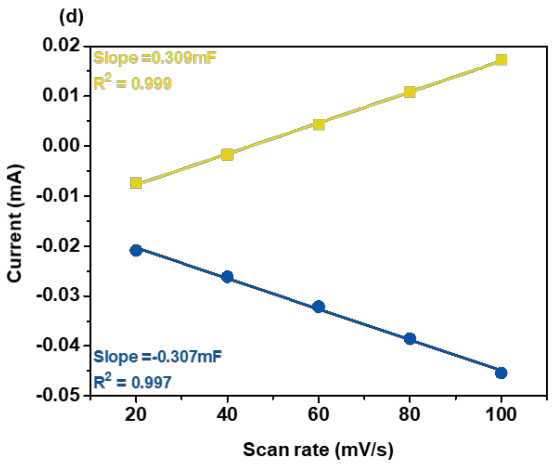
(d)
Slope =0.309mF
R2 = 0.999
Slope =-0.307mF
R2 = 0.997
Current (mA)
Scan rate (mV/s)

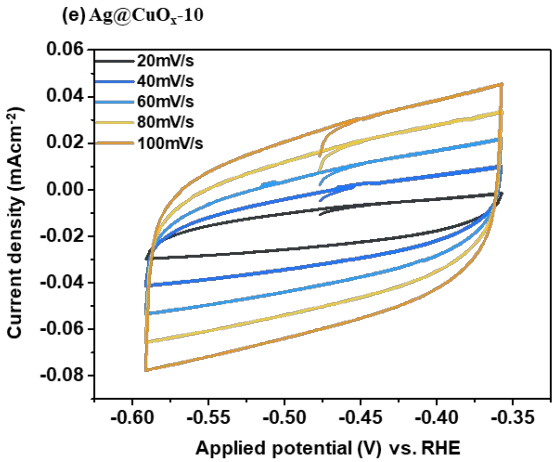
(e) Ag@CuOx-10
20mV/s
40mV/s
60mV/s
80mV/s
100mV/s
Current density (mAcm-2)
Applied potential (V) vs. RHE

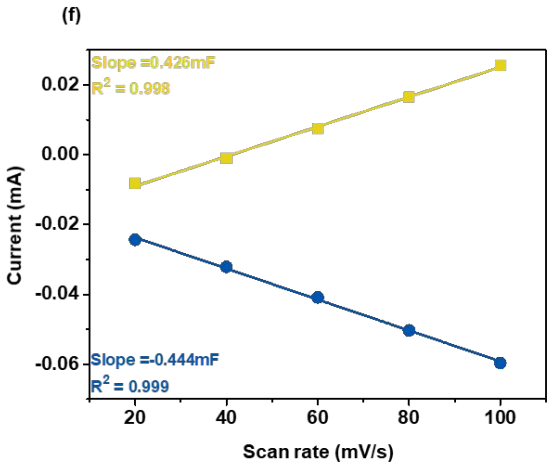
(f)
Slope =0.426mF
R2 = 0.998
Slope =-0.444mF
R2 = 0.999
Current (mA)
Scan rate (mV/s)

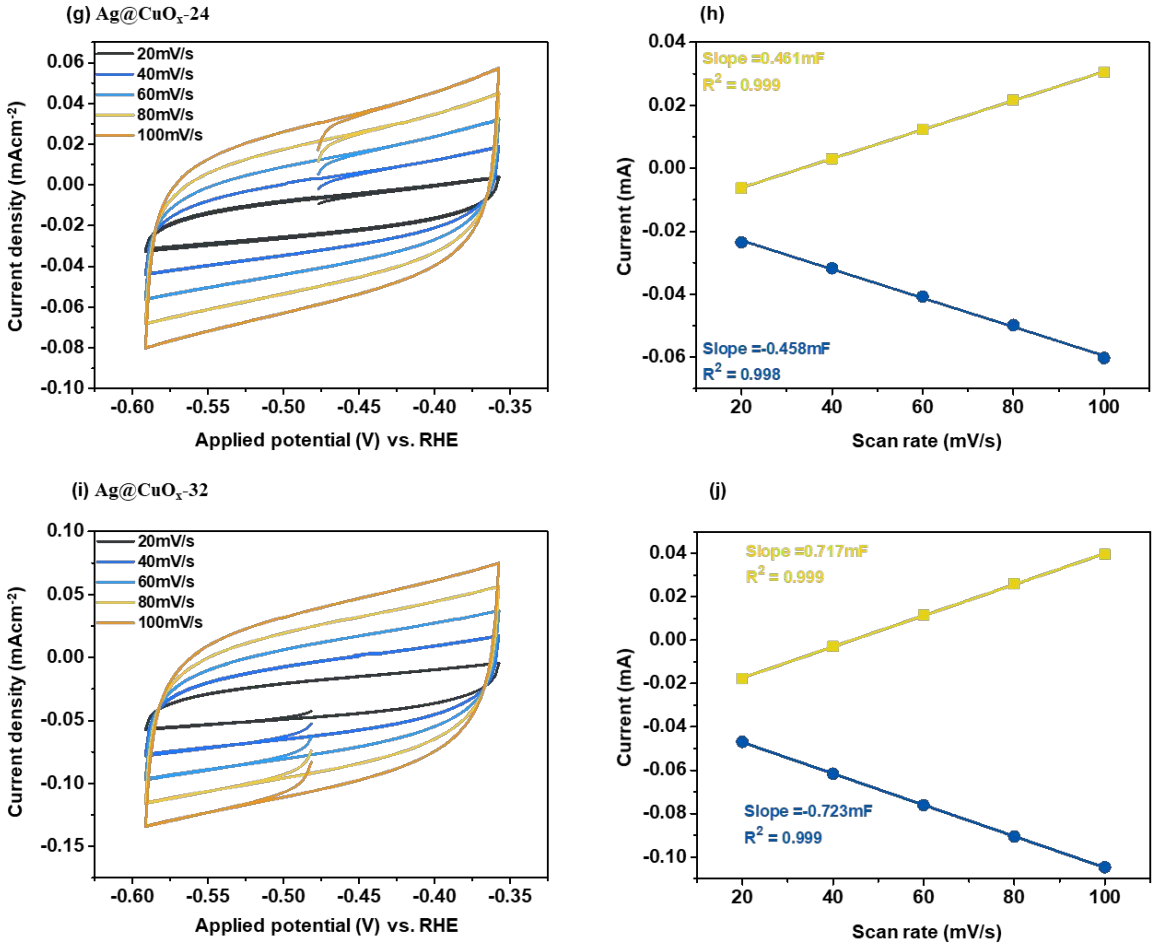

Figure S5. a, c, e, g, i show the cyclic voltammograms with different scan rate. (b, d, f, h, j) show the linear fit of anodic and cathodic charging current as a function of scan rate.

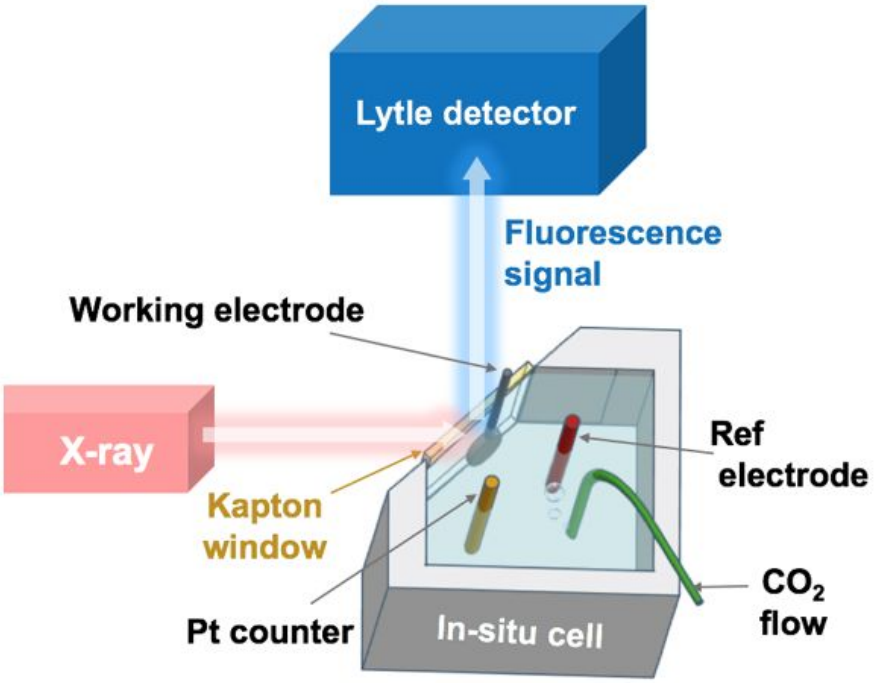

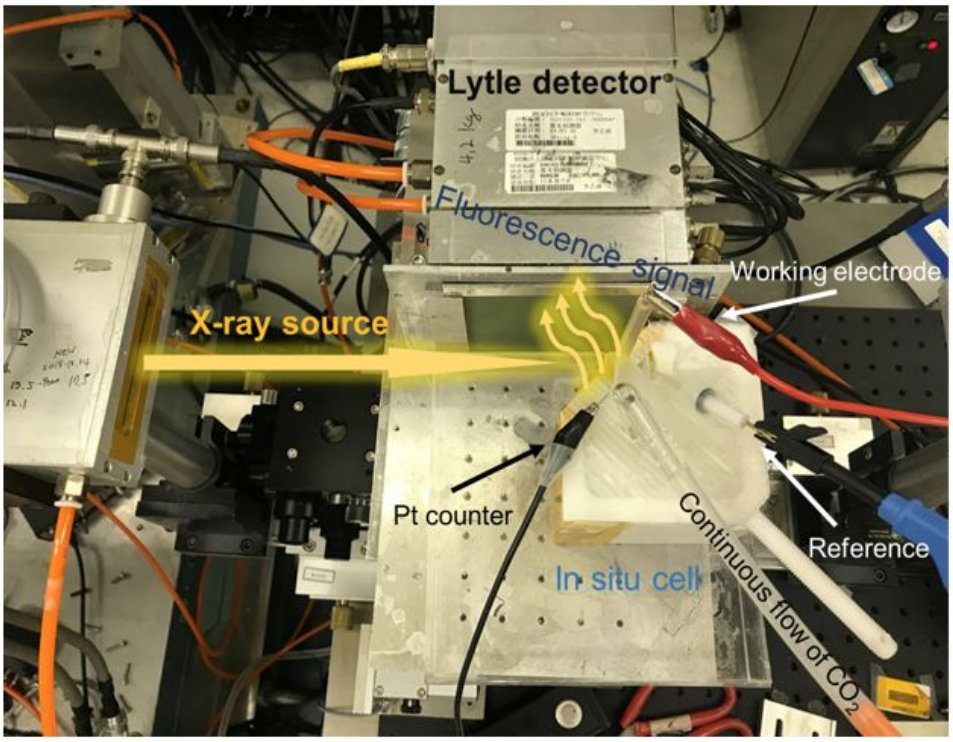

Figure S6. The setup for the *in-situ* X-ray absorption spectroscopy measurement, which was carried out at the SP8 SP12B1 beamline at SPring-8, Japan.

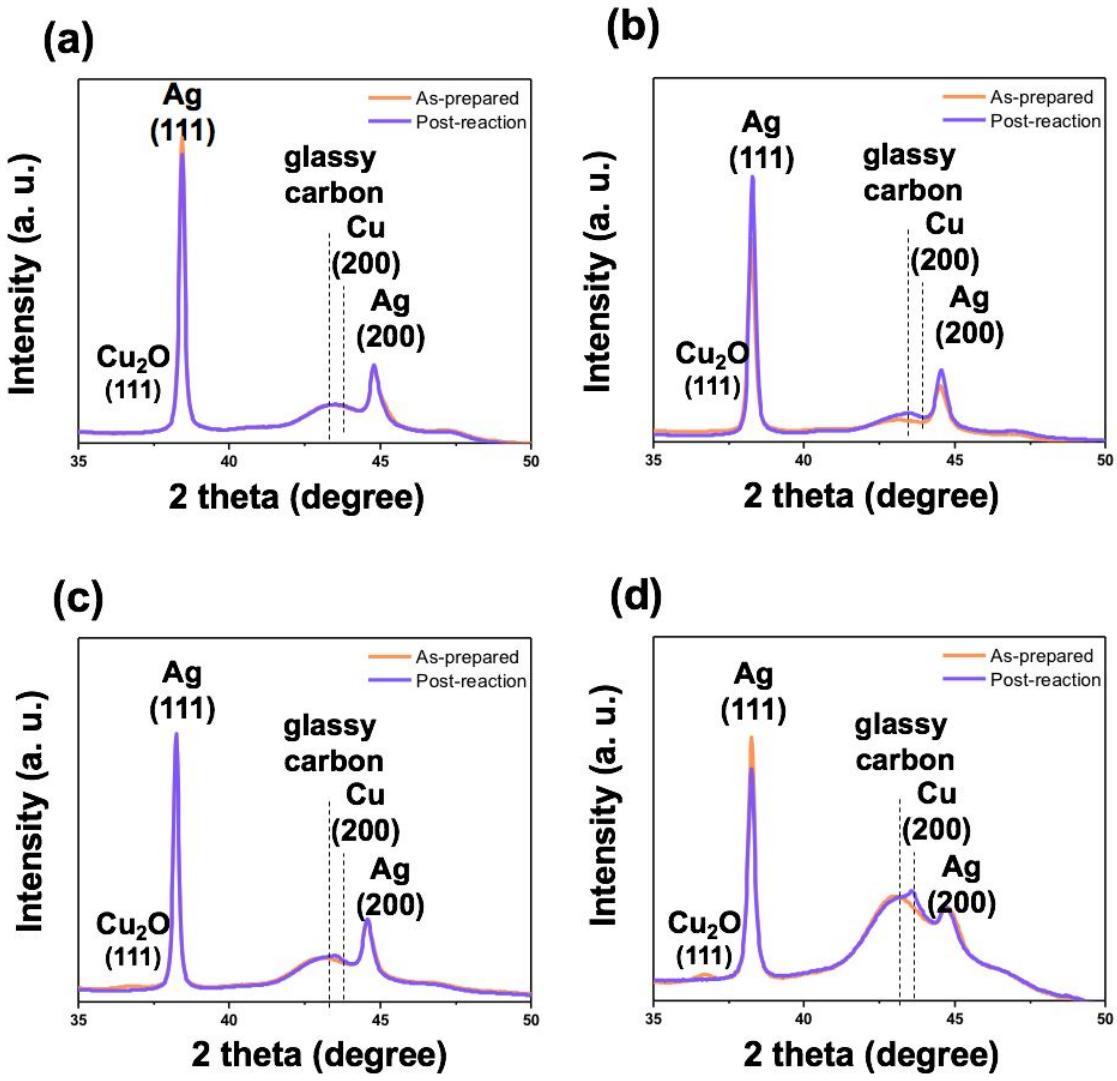

Figure S7. Grazing-angle X-ray diffraction results on the as-prepared and post-reaction samples. The characteristic peaks of Ag did not shift to higher angle after the reaction. (a) Ag@CuO_x-4, (b) Ag@CuO_x-10, (c) Ag@CuO_x-24, and (d) Ag@CuO_x-32.

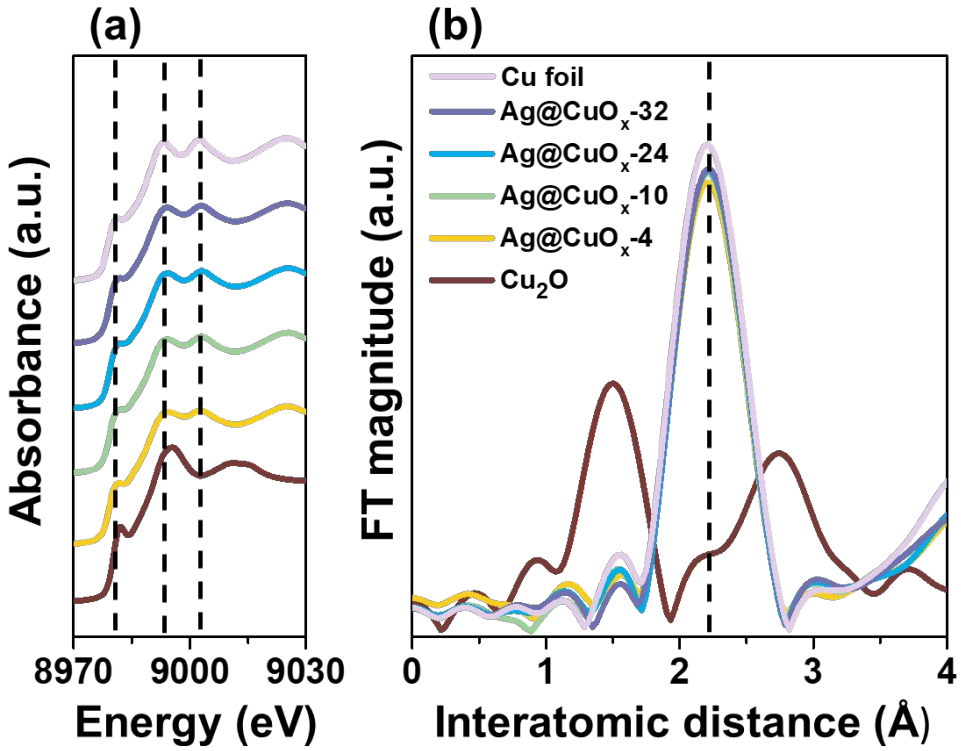

Figure S8. Cu K-edge XAS result for the post-catalysts (a) XANES and (b) EXAFS.

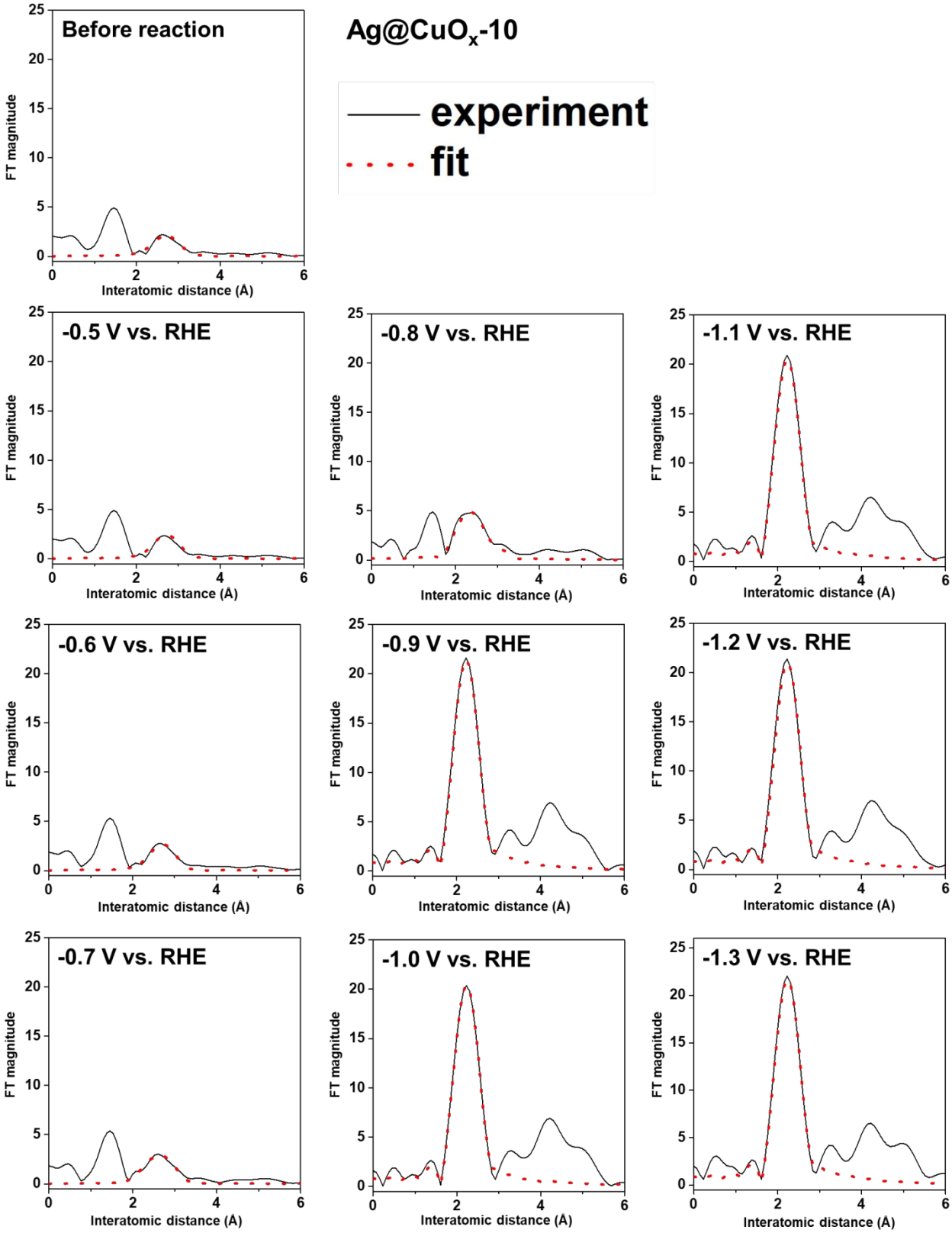

Figure S9. *In-situ* EXAFS and the fitting results of Ag@CuOx-10.

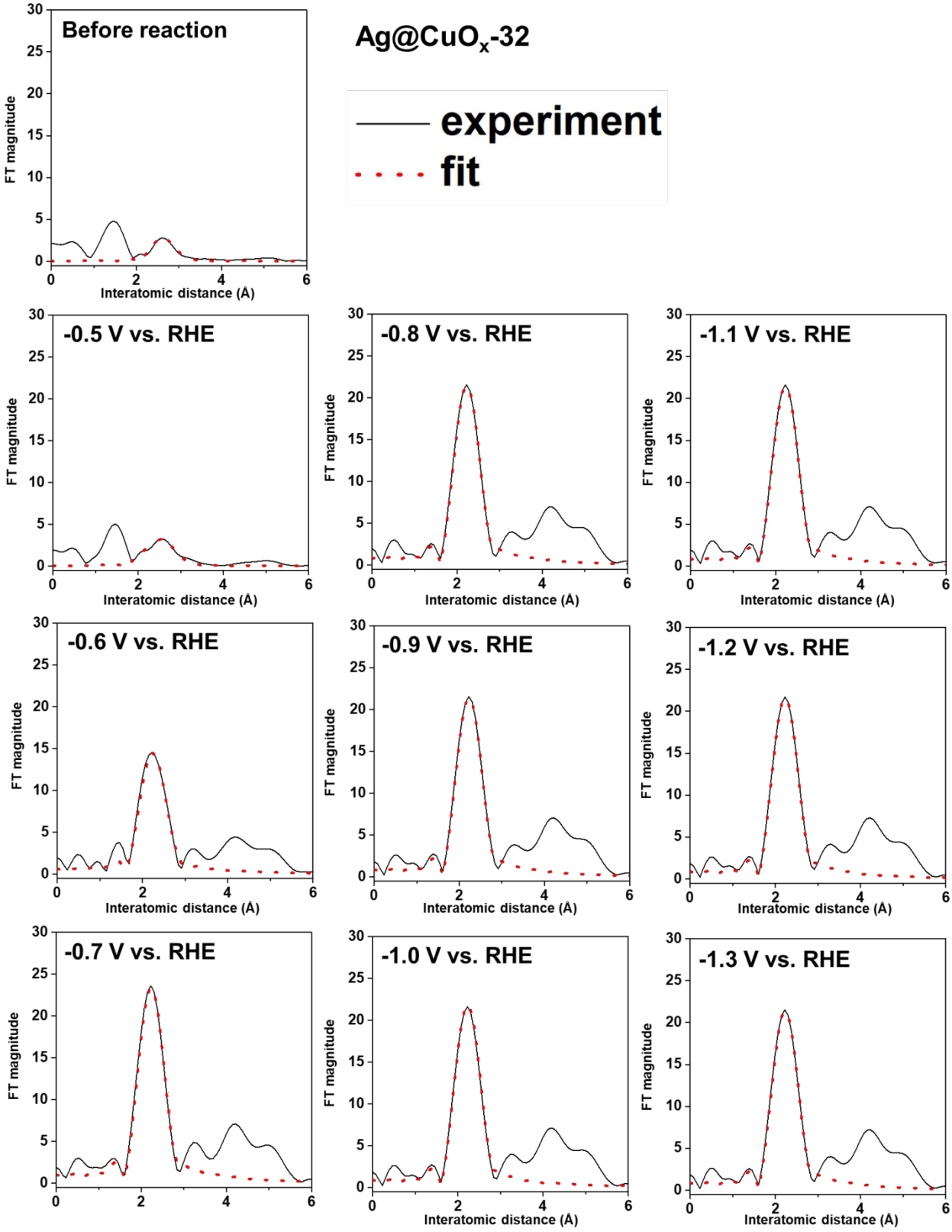

Figure S10. *In-situ* EXAFS and the fitting results of Ag@CuO_x-32.

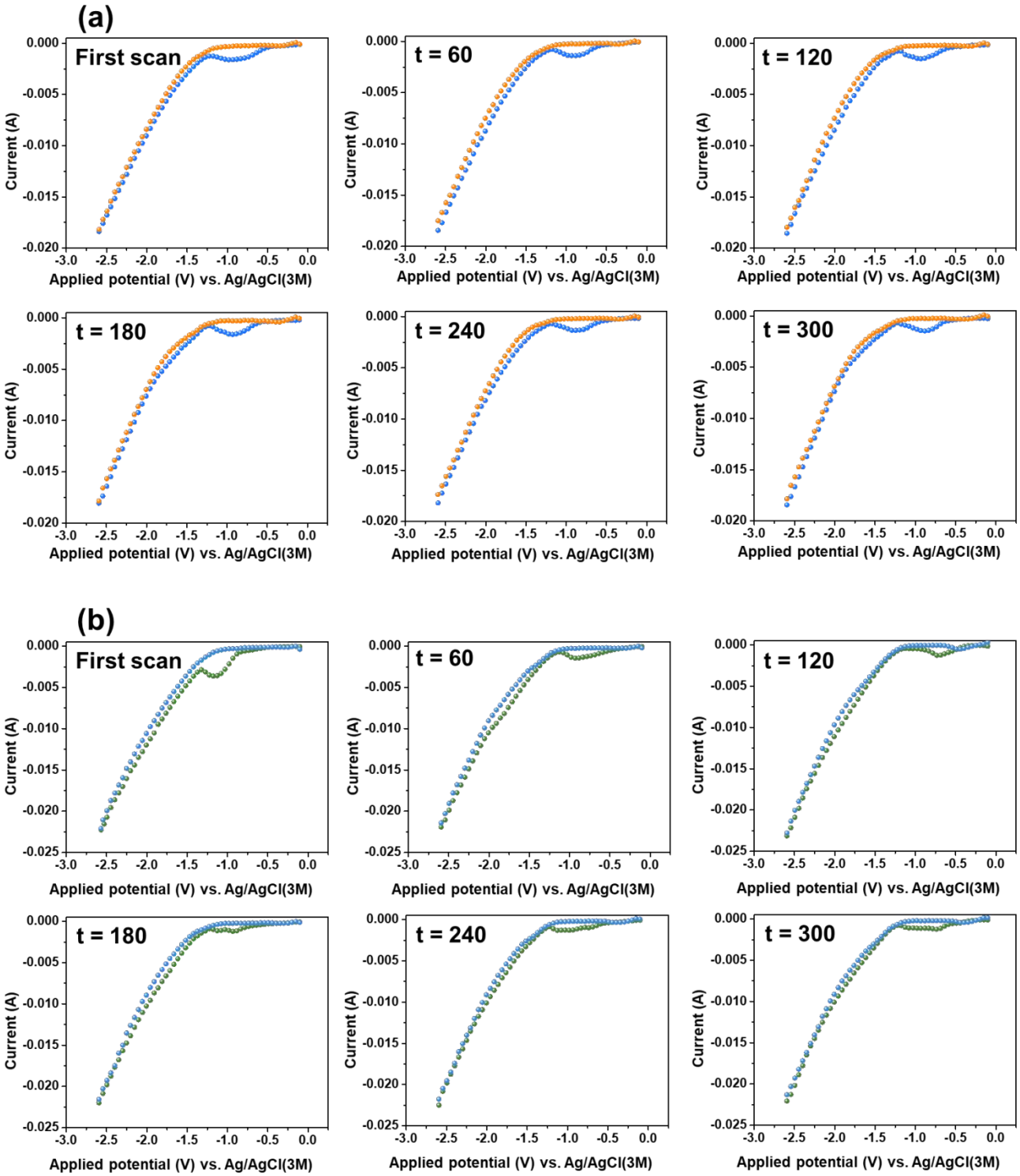

Figure S11. LSV curves examination at specific point in time. LSV with 10 mV s^{-1} for each measurement at specific point in time was proceeded two times. The second LSV curve could estimate the double-layer current in order to minimize the deviation. The total coulomb was obtained by integrating the time and the current at the potential range of the redox peak, followed by subtracting the coulomb caused by the double layer. (a) Ag@CuO_x-10 sample, and (b) Ag@CuO_x-32 sample.

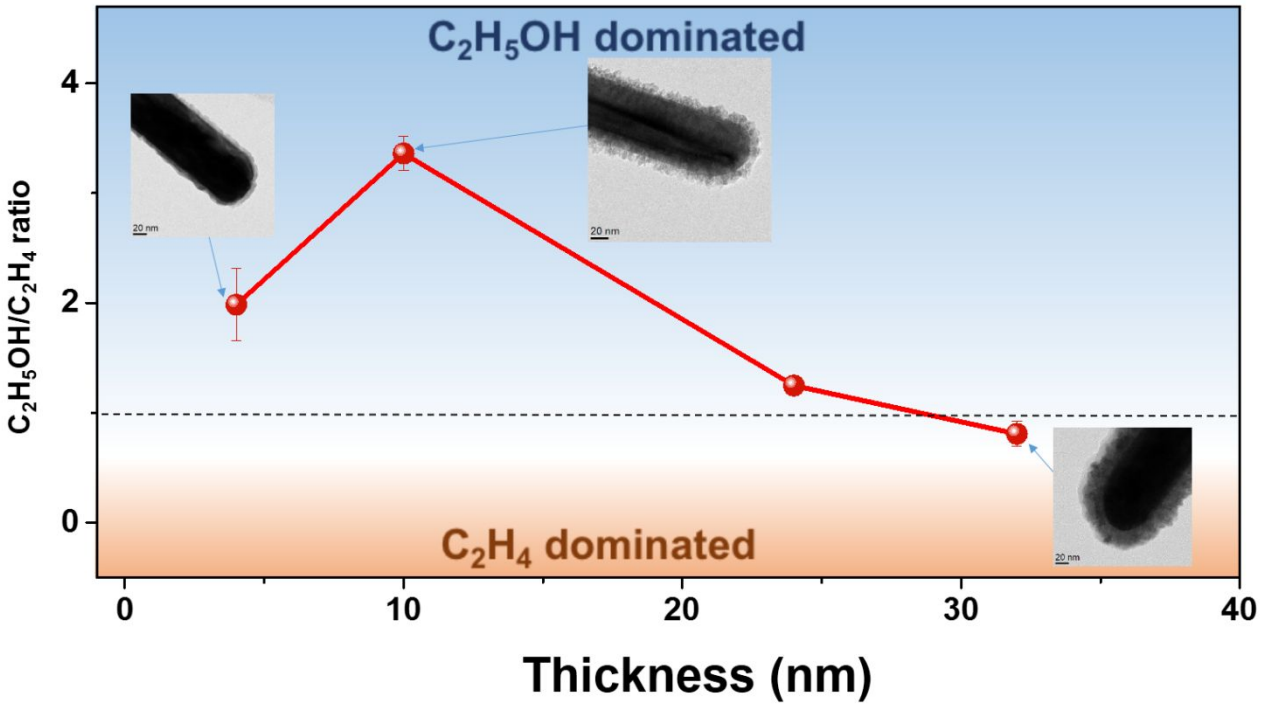

Figure S12. The ratio of ethanol to ethylene production as a function of CuO_x thickness (at -1.20 V vs. RHE).

Table S1a. Summary of double-layer capacitance from each sample.

Sample / DL capacitance (mF)	Ag nanowire	Ag@CuO_x-4	Ag@CuO_x-10	Ag@CuO_x-24	Ag@CuO_x-32
Slope from anodic charging current	0.304	0.309	0.426	0.461	0.717
Slope from cathodic charging current	-0.273	-0.307	-0.444	-0.458	-0.723
Average of the absolute value of slope	0.289	0.308	0.435	0.460	0.720

Capacitance of electropolished Cu: 0.0474 mF[1]

Table S1b. Summary of roughness factor for Ag@CuO_x-10 and Ag@CuO_x-32.

Sample	**Roughness factor (RF)**
electropolished Cu	1.00
Ag@CuO_x-10	9.17
Ag@CuO_x-32	15.18

Table S2. Faradaic efficiency distribution as a function of potential of Ag nanowire, Ag@CuO_x-4, Ag@CuO_x-10, Ag@CuO_x-24, and Ag@CuO_x-32.

Ag						
$V_{VS.\ RHE}$	**H_2 (%)**	**CO (%)**	**CH_4 (%)**	**C_2H_4 (%)**	**C_2H_5OH (%)**	**C_3H_7OH (%)**
-0.53	95.33	1.09	-	-	-	-
-0.67	67.57	28.01	-	-	-	-
-0.82	21.48	66.55	-	-	-	-
-0.93	10.74	76.22	-	-	-	-
-1.04	7.10	78.21	-	-	-	-
-1.14	5.93	76.38	-	-	-	-
-1.25	23.80	66.90	-	-	-	-
-1.30	40.85	46.20	1.85	-	-	-
-1.34	58.43	37.81	1.01	-	-	-

Ag@CuO_x-4						
$V_{VS.\ RHE}$	**H_2 (%)**	**CO (%)**	**CH_4 (%)**	**C_2H_4 (%)**	**C_2H_5OH (%)**	**C_3H_7OH (%)**
-0.54	91.86	-	-	-	-	-
-0.58	67.20	24.40	-	-	-	-
-0.68	50.60	50.88	-	-	-	-
-0.76	47.73	51.25	-	-	-	-
-0.84	42.40	58.30	-	-	-	-
-0.93	28.43	62.60	-	-	-	-
-0.98	24.49	69.72	-	-	-	-
-1.04	22.32	60.66	-	3.12	4.82	1.41
-1.16	19.12	59.38	1.32	4.58	12.17	1.99
-1.21	27.46	51.24	6.08	3.00	5.95	1.20

Ag@CuO_x-10						
$V_{VS.\ RHE}$	**H_2 (%)**	**CO (%)**	**CH_4 (%)**	**C_2H_4 (%)**	**C_2H_5OH (%)**	**C_3H_7OH (%)**
-0.48	93.47	-	-	-	-	-
-0.61	83.15	6.45	-	-	-	-
-0.74	66.17	24.24	-	-	-	-
-0.82	55.90	32.03	-	-	-	-
-0.98	47.30	47.30	-	1.59	-	-
-1.05	16.67	56.70	4.81	4.50	6.20	1.37
-1.13	20.27	23.81	15.92	13.09	18.13	3.33
-1.16	20.70	15.10	19.90	11.16	26.20	4.00
-1.20	32.70	9.96	24.90	8.36	28.08	2.42
-1.26	46.39	7.69	21.04	6.77	16.10	1.38

Ag@CuO_x-24						
$V_{VS.\ RHE}$	**H_2 (%)**	**CO (%)**	**CH_4 (%)**	**C_2H_4 (%)**	**C_2H_5OH (%)**	**C_3H_7OH (%)**
-0.49	96.00	1.08	-	-	-	-
-0.61	89.80	1.63	-	-	-	-
-0.75	86.70	2.61	-	-	-	-
-0.84	87.70	3.99	-	-	-	-
-0.92	65.69	6.44	-	2.59	1.67	1.62
-0.99	49.40	15.80	3.70	8.06	8.21	4.27
-1.02	31.10	5.33	7.20	21.30	18.76	9.92
-1.07	34.03	4.35	9.56	24.30	20.59	7.00
-1.11	38.60	0.00	10.96	20.55	24.42	5.80
-1.20	52.58	0.00	11.49	15.31	19.10	4.40

Ag@CuO$_x$-32						
$V_{VS.\ RHE}$	**H_2 (%)**	**CO (%)**	**CH_4 (%)**	**C_2H_4 (%)**	**C_2H_5OH (%)**	**C_3H_7OH (%)**
-0.46	100.15	-	-	-	-	-
-0.63	86.10	3.56	-	-	-	-
-0.79	72.60	9.75	-	-	-	-
-0.87	63.02	8.81	-	2.62	2.01	0.95
-0.97	38.28	9.02	1.02	10.66	8.75	6.26
-1.02	24.62	6.44	2.54	26.42	16.58	11.18
-1.06	22.96	3.55	3.75	31.55	18.69	10.51
-1.12	40.78	2.17	7.15	28.58	19.95	6.95
-1.23	39.26	1.42	10.93	25.58	20.75	5.60
-1.27	46.90	0.00	10.34	20.33	19.64	3.38

Table S3. Fitting parameters for Ag@CuO_x-10.

condition	path	N	R (Å)	ΔE (eV)	σ^2 (Å^2)
Before reaction	Cu foil Cu-Cu	-	-	-	-
	Cu_2O Cu-Cu	8.9(5)	3.00(2)	6.9(4)	0.0158(6)
-0.50 V vs. RHE	Cu foil Cu-Cu	-	-	-	-
	Cu_2O Cu-Cu	8.7(5)	3.01(3)	7.7(4)	0.0151(1)
-0.60 V vs. RHE	Cu foil Cu-Cu	-	-	-	-
	Cu_2O Cu-Cu	8.7(4)	3.01(2)	6.8(4)	0.0147(5)
-0.70 V vs. RHE	Cu foil Cu-Cu	0.5(1)	2.54(3)	3.2(9)	0.0090(9)
	Cu_2O Cu-Cu	8.5(4)	3.01(3)	6.8(4)	0.0145(5)
-0.80 V vs. RHE	Cu foil Cu-Cu	1.8(2)	2.54(2)	2.1(4)	0.0076(4)
	Cu_2O Cu-Cu	7.3(4)	3.02(4)	7.4(5)	0.0146(5)
-0.90 V vs. RHE	Cu foil Cu-Cu	10.8(5)	2.53(3)	2.4(2)	0.0084(6)
	Cu_2O Cu-Cu	-	-	-	-
-1.00 V vs. RHE	Cu foil Cu-Cu	11.2(3)	2.54(4)	2.8(5)	0.0088(8)
	Cu_2O Cu-Cu	-	-	-	-
-1.10 V vs. RHE	Cu foil Cu-Cu	11.3(8)	2.54(5)	2.5(4)	0.0088(9)
	Cu_2O Cu-Cu	-	-	-	-
-1.20 V vs. RHE	Cu foil Cu-Cu	11.3(8)	2.53(4)	2.8(4)	0.0087(7)
	Cu_2O Cu-Cu	-	-	-	-
-1.30 V vs. RHE	Cu foil Cu-Cu	11.3(6)	2.54(3)	2.8(3)	0.0085(2)
	Cu_2O Cu-Cu	-	-	-	-

Table S4. Fitting parameters for Ag@CuO_x-32.

condition	path	N	R (Å)	ΔE (eV)	σ^2 ($Å^2$)
Before reaction	Cu foil Cu-Cu	0.4(2)	2.54(2)	-14.2(9)	0.0098(9)
	Cu_2O Cu-Cu	8.6(5)	2.97(5)	4.1(7)	0.0155(6)
-0.50 V vs. RHE	Cu foil Cu-Cu	1.0(6)	2.54(4)	-1.4(9)	0.0088(8)
	Cu_2O Cu-Cu	8.4(5)	2.99(5)	6.4(6)	0.0156(6)
-0.60 V vs. RHE	Cu foil Cu-Cu	5.9(6)	2.54(7)	1.8(1)	0.0072(4)
	Cu_2O Cu-Cu	1.3(7)	3.01(6)	9.9(7)	0.0098(9)
-0.70 V vs. RHE	Cu foil Cu-Cu	11.1(7)	2.54(8)	2.6(7)	0.0081(5)
	Cu_2O Cu-Cu				
-0.80 V vs. RHE	Cu foil Cu-Cu	11.5(7)	2.54(7)	2.4(5)	0.0087(6)
	Cu_2O Cu-Cu				
-0.90 V vs. RHE	Cu foil Cu-Cu	11.5(8)	2.54(6)	2.4(6)	0.0087(5)
	Cu_2O Cu-Cu				
-1.00 V vs. RHE	Cu foil Cu-Cu	11.5(7)	2.54(7)	2.4(7)	0.0086(3)
	Cu_2O Cu-Cu				
-1.10 V vs. RHE	Cu foil Cu-Cu	11.5(6)	2.54(5)	2.5(5)	0.0087(6)
	Cu_2O Cu-Cu				
-1.20 V vs. RHE	Cu foil Cu-Cu	11.5(8)	2.54(6)	2.5(2)	0.0087(7)
	Cu_2O Cu-Cu				
-1.30 V vs. RHE	Cu foil Cu-Cu	11.5(7)	2.54(7)	2.5(3)	0.0087(8)
	Cu_2O Cu-Cu				

Table S5. Previous reports showed that the Cu^+ existed through various techniques.

	technique	result	reference
●	operando XAS	Cu^+ species	1
●	quasi *in-situ* XPS	Cu^+ species~13 at%	2
●	*ex-situ* AES and XAS	Mixed copper states	3
●	quasi *in-situ* TEM and PAS	Subsurface oxygen	4
●	*in-situ* XAS	Cu^+ ~23 %	5
●	*in-situ* XAS	Avg. Oxidation State of Cu: +0.32	6
●	*in-situ* XAS	Partial reduction of Cu_2O to Cu	7

References

1. Mistry, H.; Varela, A. S.; Bonifacio, C. S.; Zegkinoglou, I.; Sinev, I.; Choi, Y. W.; Kisslinger, K.; Stach, E. A.; Yang, J. C.; Strasser, P.; Cuenya, B. R., Highly Selective Plasma-Activated Copper Catalysts for Carbon Dioxide Reduction to Ethylene. *Nat. Commun.* **2016,** *7*, 12123.
2. Gao, D.; Zegkinoglou, I.; Divins, N. J.; Scholten, F.; Sinev, I.; Grosse, P.; Roldan Cuenya, B., Plasma-Activated Copper Nanocube Catalysts for Efficient Carbon Dioxide Electroreduction to Hydrocarbons and Alcohols. *ACS Nano* **2017,** *11*, 4825-4831.
3. Lee, S. Y.; Jung, H.; Kim, N.-K.; Oh, H.-S.; Min, B. K.; Hwang, Y. J., Mixed Copper States in Anodized Cu Electrocatalyst for Stable and Selective Ethylene Production from CO_2 Reduction. *J. Am. Chem. Soc.* **2018,** *140*, 8681-8689.
4. Cavalca, F.; Ferragut, R.; Aghion, S.; Eilert, A.; Diaz-Morales, O.; Liu, C.; Koh, A. L.; Hansen, T. W.; Pettersson, L. G. M.; Nilsson, A., Nature and Distribution of Stable Subsurface Oxygen in Copper Electrodes During Electrochemical CO_2 Reduction. *J. Phys. Chem. C* **2017,** *121*, 25003-25009.
5. De Luna, P.; Quintero-Bermudez, R.; Dinh, C.-T.; Ross, M. B.; Bushuyev, O. S.; Todorović, P.; Regier, T.; Kelley, S. O.; Yang, P.; Sargent, E. H., Catalyst Electro-Redeposition Controls Morphology and Oxidation State for Selective Carbon Dioxide Reduction. *Nat. Catal.* **2018,** *1*, 103-110.
6. Zhou, Y.; Che, F.; Liu, M.; Zou, C.; Liang, Z.; De Luna, P.; Yuan, H.; Li, J.; Wang, Z.; Xie, H.; Li, H.; Chen, P.; Bladt, E.; Quintero-Bermudez, R.; Sham, T.-K.; Bals, S.; Hofkens, J.; Sinton, D.; Chen, G.; Sargent, E. H., Dopant-Induced Electron Localization Drives CO_2 Reduction to C_2 Hydrocarbons. *Nat. Chem.* **2018,** *10*, 974-980.
7. Lee, S.; Kim, D.; Lee, J., Electrocatalytic Production of C_3-C_4 Compounds by Conversion of CO_2 on a Chloride-Induced Bi-Phasic Cu_2O-Cu Catalyst. *Angew. Chem. Int. Ed.* **2015,** *127*, 14914-14918.